# Solution Structure of Metal Particles Prepared in Unimolecular Reactors of Amphiphilic Hyperbranched Macromolecules

**ARTICLE** *in* MACROMOLECULES · SEPTEMBER 2004

Impact Factor: 5.8 · DOI: 10.1021/ma048965g · Source: OAI



**7 AUTHORS**, INCLUDING:

Vasil M Garamus
Helmholtz-Zentrum Geesthacht
**223** PUBLICATIONS **2,535** CITATIONS
SEE PROFILE

Walter Richtering
RWTH Aachen University
**237** PUBLICATIONS **6,060** CITATIONS
SEE PROFILE

Cyril Aymonier
French National Centre for Scientific Research
**137** PUBLICATIONS **2,138** CITATIONS
SEE PROFILE

# Solution Structure of Metal Particles Prepared in Unimolecular Reactors of Amphiphilic Hyperbranched Macromolecules

**Vasil M. Garamus**

*GKSS Research Centre, Max Planck Str., D-21502 Geesthacht, Germany*

**Tatiana Maksimova and Walter Richtering***

*RWTH Aachen University, Institut für Physikalische Chemie, Templergraben 59, D-52056 Aachen, Germany*

**Cyril Aymonier and Ralf Thomann**

*Institut für Makromolekulare Chemie und Freiburger Materialforschungszentrum der Albert-Ludwigs-Universität Freiburg, Stefan-Meier-Str. 31, D-79104 Freiburg, Germany*

**Lydie Antonietti and Stefan Mecking***

*Universität Konstanz, Fachbereich Chemie, Universitätsstr. 10, D-78457 Konstanz, Germany*

*Received May 25, 2004; Revised Manuscript Received August 9, 2004*

ABSTRACT: The structure of metal nanoparticles templated by amphiphilic hyperbranched polyethylenimine-amides in apolar organic solution was studied by means of small-angle neutron scattering (SANS). SANS measurements at different concentrations revealed that the neat polymer is present as nonaggregated unimolecular micelles for a polymer with $M_w$ 3.9 × $10^4$ g $mol^{-1}$ and that silver particles are stabilized by a single polymer molecule. For a polymer of $M_w$ 1.2 × $10^4$ g $mol^{-1}$, some aggregation occurs upon loading with the silver salt ($AgNO_3$) and particle formation. Contrast variation experiments were performed employing different compositions of $C_6D_6$ and $C_6H_6$ in the solvent mixture. For the larger molar mass polymer a homogeneous distribution is found for the polymer/metal particle hybrides, whereas for the lower molecular weight polymer the metal particles are off-center.

## Introduction

The synthesis of metal colloids and their properties have drawn considerable attention for more than a century.[1] They are usually prepared by reduction of metal salts in the presence of suitable low-molecular-weight or polymeric stabilizers[1] or electrochemically,[2] and decomposition of organometallic precursors[3] has also been investigated intensively. Whereas the larger part of this work has focused on aqueous colloids, metal colloids in organic solvents are also well-known. The latter is of particular interest, e.g., for catalysis. Despite the long-lasting interest in this topic, facile syntheses of stable metal colloids with controlled particle size remain a challenge.

A topic that has found considerable attention only in recent years is the control of particle sizes by means of synthesis in a confined environment. A predetermined amount of metal precursor molecules ions can be located inside a "nanoreactor", where they are reduced to exactly one metal particle per reactor. This concept has been suggested for metal particle synthesis in "polymerized micelles" early on.[4] For linear block copolymer micelles containing a coordinating block as the micelle core, a single metal particle can be prepared per micelle under suitable conditions.[5,6] The resulting colloids can be used to arrange monodisperse gold nanoparticles on a surface in regular, controlled distances for example.

Block copolymer micelles are by their very nature dynamic structures, and aggregation numbers can be subtly dependent on reaction conditions; moreover, such structures can be shear-sensitive. Therefore, unimolecular micelles as "nanoreactors" are of interest. To this end, the concept of amphiphilic macromolecules with a highly branched polar scaffold as a core and apolar moieties on their periphery appears attractive. Such polymers can be soluble in apolar organic solvents, possibly forming unimolecular inverted micelles.

The polar scaffold can take up and coordinate metal precursors for particle synthesis and subsequently interact with the particles formed and bind them in the interior of the macromolecule. Indeed, (nonamphiphilic, water-soluble) dendrimers stabilize metal particles in aqueous solution very effectively.[7,8] While the formation of one metal particle per dendrimer has been claimed previously, to our understanding clear experimental proof was provided only for one particular case by Amis et al.[9] Charged poly(amidoamine) (PAMAM) dendrimers formed by protonation of PAMAM with $H[AuCl_4]$ upon reduction of the gold compound afforded one gold nanoparticle stabilized by one dendrimer molecule only in the range of generations G6−G9.

As a highly branched dendritic scaffold for the aforementioned unimolecular inverted micelle concept, dendrimers[10] or hyperbranched polymers[11] can be considered. By comparison to the ideally perfectly branched dendrimers (degree of branching,[12] DB = 100%), hyperbranched polymers possess a randomly branched topology (degree of branching, DB ca. 60%). Unlike the tedious multistep syntheses of dendrimers, hyperbranched polymers can be obtained by single-step protocols, making them attractive for applications.

* Corresponding authors. E-mail: richtering@rwth-aachen.de; stefan.mecking@uni-konstanz.de.

10.1021/ma048965g CCC: $27.50 
Published on Web 09/25/2004

Although they are not monodisperse like dendrimers, certain hyperbranched polymers can be prepared conveniently with narrow molecular weight distributions. Hyperbranched polyethylenimine and polyglycerol are commercially available with narrow molecular weight distributions.[13,14]

Amphiphilically modified dendrimers[15,16] as well as amphiphilically modified hyperbranched polyglycerols[17−20] or polyethylenimines[20,21] effectively stabilize metal nanoparticles in apolar solvents. Concerning the concept of particle synthesis and stabilization in unimolecular nanoreactors, supporting or contradictive experimental evidence is lacking. In view of the flexible nature of dendritic scaffolds employed, formation of aggregates of a large number of molecules in solution is equally well conceivable as a unimolecular micelle behavior. For investigations of the solution structures of hybrids of highly branched amphiphiles with metal particles, modified polyethylenimines are more suited than polyglycerols, as the amine functions of the branched scaffold coordinate more strongly than the polyether−polyol scaffold of the polyglycerols.

We now report for the first time on the solution structure of hybrids of metal particle with highly branched amphiphiles. As a model system, hybrids of silver nanoparticles with hyperbranched polyethylenimine-amide were investigated by small-angle neutron scattering (SANS).

## Experimental Section

**Materials**. Polyethylenimine (PEI) was dried prior to use by stirring for several days at 100 °C under vacuum (<1 mbar). Methyl palmitate (97%) and silver nitrate (≥99.5%) were obtained from Fluka.

**Polymer Synthesis**. To a 250 mL glass reactor equipped with a mechanical stirrer, a reflux condensor connected with a membrane vacuum pump, and a thermocouple dipping into the reaction mixture, the required amounts of polyethylenimine (e.g., 5.0 g; corresponding to an overall 0.116 mol of N) and methyl palmitate (9.4 g; 0.035 mol) were added. The mixture was heated by means of an oil bath and stirred at 140 °C under vacuum for 20 h, affording the PEI-amide. If present, impurities of unreacted ester (indicated by the $^{13}$C NMR signals of $CH_2C(O)$) can be removed by ultrafiltration in toluene solution on a Koch MPF-50 membrane (nominal molecular weight cutoff 700 Da). The aforementioned example afforded a polymer of degree of amidation 43% (vide supra for definition of degree of amidation).

Inverse gated $^{13}$C NMR of the starting material PEI shows the PEI core to consist of around 30% of primary amine moieties (end groups), 40% of secondary amines (linear units), and 30% of tertiary amines (branching points). The degrees of amidation of the PEI-amides were determined by $^1$H NMR from the signals of the PEI backbone (2.4−4 ppm) and the signals of the $C_{15}H_{31}$ alkyl chains (0.8−2.1 ppm). A polymer with 40% degree of amidation prepared from a $5 \times 10^3$ g mol$^{-1}$ PEI core ("5K") is abbreviated, for example, as PEIam5K$^{lin}$-C16$_{0.4}$ ($^{lin}$C16 standing for palmitic amide, i.e., derived from the linear fatty acid with 16 carbon atoms). A degree of amidation of 100% corresponds to complete conversion of secondary amines $R_2NH$ and primary amines $RNH_2$ to $R_2NC(=O)C_{15}H_{31}$ and $RNHC(=O)C_{15}H_{31}$ (R = polymer scaffold), respectively. It can be noted that $^{13}$C NMR of the PEI-amides reveals that when a corresponding limited amount of palmitic acid derivative is employed, the primary amine groups (end groups) are amidated nearly selectively (complete disappearance of the $CH_2CH_2NH_2$ peaks at 41.4 and 39.5). Thus, a degree of amidation of 43% corresponds approximately to full amidation of all primary amine groups, whereas the secondary amine groups remain largely unreacted.

A full account of polymer synthesis and properties will also be published elsewhere.[22]

**Metal Colloid Synthesis.** Solutions of the polymers in deuterated benzene (10 g L$^{-1}$) were stirred at room temperature with silver nitrate (1 $Ag^+$ per 4 N atoms; that is e.g. 3.3 g L$^{-1}$ for a polymer of 50% degree of amidation) under an argon atmosphere. Silver nitrate, which is not soluble in benzene in the absence of the polymer, is solubilized by the polymer upon stirring overnight to afford clear yellow solutions. The corresponding polymer solutions, which were also investigated by SANS in some cases, are designated e.g. as PEIam5K$^{lin}$C16$_{0.5}$/$Ag^+$. For the synthesis of colloids, after stirring the solutions overnight, reduction was performed under a hydrogen atmosphere (1.5 bar) for another 48 h. The corresponding colloids are designated e.g. as PEIam5K$^{lin}$C16$_{0.5}$/Ag$^{coll}$. Sizes of the metal nanoparticles were determined by transmission electron microscopy (TEM) on a LEO 912 Omega microscope at an acceleration voltage of 120 kV. For PEIam5K$^{lin}$C16$_{0.5}$/Ag$^{coll}$ an average particle size of 1.2 ± 0.3 nm and for PEIam25K$^{lin}$-C16$_{0.5}$/Ag$^{coll}$ an average particle size of 2.3 ± 0.4 nm were determined (cf. Supporting Information).

**Polymer Density Determination**. The densities of the two polymers were determined with a digital instrument by Anton Paar KG, which is based on the variation of the resonance frequency of a piezo element depending on the density of the surrounding medium. Measurements were performed on a series of polymer solutions in $C_6D_6$ with varying concentrations (0.5−1.5 wt %) at 20 °C (cf. Supporting Information). For PEIam5K$^{lin}$C16$_{0.5}$ a density of 0.95 ± 0.01 g L$^{-1}$ and for PEIam25K$^{lin}$C16$_{0.5}$ a density of 0.96 ± 0.01 g L$^{-1}$ was determined.

**SANS Measurements.** Small-angle neutron scattering experiments were performed with the SANS1 instrument at the FRG1 research reactor at the GKSS Research Center, Geesthacht, Germany.[23] The neutron wavelength was 8.1 Å with a wavelength resolution of 10% (fwhm). A range of scattering vectors $0.007 < q < 0.25$ Å$^{-1}$ was obtained using three sample-to-detector distances (0.7−7 m). Samples were kept at 25 ± 1 °C in quartz cuvettes with a path length of 1 mm. Raw spectra were corrected for backgrounds from solvent, sample cell, and other sources by conventional procedures. The two-dimensional isotropic scattering spectra were azimuthally averaged, converted to an absolute scale, and corrected for detector efficiency by dividing by the incoherent scattering spectrum of pure water, which was measured with a 1 mm cell.

For each instrumental setting, the scattering curves were smeared by the appropriate resolution function. The calculated scattering intensity was fitted to the experimental results by means of least-squares analysis, and the errors of parameters were calculated by conventional methods.[24−26] Contrast variation experiments were performed using mixtures of $C_6D_6$ and $C_6H_6$ at different compositions in the range 1/0 to 1/1.

**Analysis of SANS Data.** The expression for the differential cross sections of neutron scattering per unit volume $d\Sigma(q)/d\Omega$, vs scattering vector $q = (4\pi/\lambda)\sin(\theta/2)$ ($\lambda$ is the wavelength and $q$ is the scattering angle) can be written as

$$d\Sigma(q)/d\Omega = nP(q)\,S(q) \qquad (1)$$

where $n$ is the number density of particles, $P(q)$ expresses the scattering cross section of one particle, and $S(q)$ is the structure factor describing the long-range organization between the particles in solution. For dilute solutions there are usually no such correlations; thus, $S(q) = 1$, and the scattering curves are determined only by structure of studied aggregates.

SANS data can be analyzed on different levels of sophistication. The scattering intensity at zero angle, $d\Sigma(0)/d\Omega$, and the $z$-average of the radius of gyration ($R_g = \langle s^2\rangle_z^{1/2}$) of the polymers can be obtained within the Guinier approximation as

$$\frac{d\Sigma(q)}{d\Omega} = \frac{d\Sigma(0)}{d\Omega}\exp(-q^2\langle s^2\rangle_z/3) \qquad (2)$$

and the weight-average molar mass $M_w$ can be obtained from

the forward scattering. The angular dependence of the scattering provides information on the shape of the particles, and many different form factors have been calculated. Burchard[27] described form factors for branched polymers that have recently been applied for the analysis of SANS data of hyperbranched polymers.[28]

More detailed information can be obtained from neutron scattering when the contrast variation approach is applied.[29] This technique was employed here in order obtain information on the internal structure of polymer and polymer/$Ag^{coll}$ hybrids. In this approach the neutron scattering length density of the solvent is varied systematically by employing mixtures of deuterated and nondeuterated solvents. This gives rise to changes in scattering, i.e., absolute intensities and the shape of the curve. The parameters of scattering intensities (scattering at "zero angle" and radius of gyration) derived from the recorded data are further analyzed to obtain an average neutron scattering length density of the investigated aggregates and a distribution of scattering length density within the aggregates.

There are two possible ways for data analysis: model independent or direct fitting of scattering curves by chosen model (Guinier's approximation, Zimm's plot, or Burchard's model).[30] In present studies we have used a model-independent analysis, i.e., indirect Fourier transformation method (IFT) which does not demand any a priori information about the structure of studied aggregates.[31]

The overall shape and dimensions of studied aggregates can be estimated from the pair distribution function $p(r)$. The scattering intensities are written in the way of pair distribution function by Fourier transform which for an isotropic sample can be expressed as

$$d\Sigma(q)/d\Omega = 4\pi\int_0^\infty p(r)\frac{\sin qr}{qr}\,dr \tag{3}$$

The pair distribution function is connected with the contrast $\Delta\rho(r)$ (difference between scattering length density of aggregate at point $r$, $\rho(r)$) and averaged scattering length density of solvent $\rho_s$, $\Delta\rho(r) = \rho(r) - \rho_s$, via an autocorrelation function of contrast

$$p(r) = r^2\int \Delta\rho(u)\,\Delta\rho(r+u)u^2\,du \tag{4}$$

The pair distribution function of an aggregate with finite maximum dimension $D_{max}$ is approximated by a linear combination of a finite number, $N$, of cubic $B$-splines, evenly distributed in the interval [0, $D_{max}$]:

$$p(r) = \sum_{i=1}^{N} a_i\varphi_i(r) \tag{5}$$

where $a_i$ is the coefficient of the $i$th cubic $B$-spline $\varphi_i(r)$. The $a_i$ coefficients are fitting parameters which are optimized using a least-squares method of minimization together with smoothness constraint.

The upper limit of the $r$ value included in the indirect Fourier transformation is chosen so that the $p(r)$ converges smoothly to $p(r) = 0$ at high $r$ values. Doing this carefully, it is possible to estimate the pair distance distribution functions of the system without particle interaction.

From $p(r)$ we can calculate integral parameters of the scattering curves,[32] forward scattered intensity $d\Sigma(0)/d\Omega$ by population of all aggregates, and the radius of gyration $R_g$ of one aggregate which is given by

$$R_{CS,g} = \left[\frac{\int_0^D r^2 p(r)\,dr}{\int_0^D p(r)\,dr}\right]^{1/2} \tag{6}$$

The forward scattered intensity (scattering at "zero angle") $d\Sigma(0)/d\Omega$ is given by

$$d\Sigma(0)/d\Omega = 4\pi\int_0^D p(r)\,dr \tag{7}$$

The above-mentioned procedure of IFT is applied for scattering data obtained at different solvents, i.e., solvents with different scattering length densities. A set of $d\Sigma(0)/d\Omega$ and $R_g$ values, which are functions of $\rho_s$, is obtained.

Within the contrast variation approach the contrast $\Delta\rho(r)$ in point $r$ of particle is written as a sum of homogeneous and inhomogeneous contributions[25]

$$\Delta\rho(r) = \langle\Delta\rho\rangle\rho_c(r) + \rho_f(r) \tag{8}$$

where $\langle\Delta\rho\rangle$ is the mean scattering contrast ($\langle\Delta\rho\rangle = \langle\rho\rangle - \rho_s$, $\langle\rho\rangle$ average scattering length density of particle), $\rho_c(r)$ is the function that describes the region that is forbidden to the solvent that is the so-called function of shape of particles, and $\rho_c(r)$ is equal to 1 inside the particle and is equal to 0 outside. The condition $\langle\Delta\rho\rangle = 0$ is called the contrast match point.

The function $\rho_f(r)$ provides a description of the structure of internal inhomogenities (fluctuations) within the aggregates and is defined as $\rho_f(r) = \rho(r) - \langle\rho\rangle$ and $\int\rho_s(r)\,dv$ within the volume of particle is equal to 0.

The scattered intensity $d\Sigma(q)/d\Omega$ corresponding to the scattering contrast (8) consists of three basic scattering functions[29] as

$$d\Sigma(q,\langle\Delta\rho\rangle)/d\Omega = \langle\Delta\rho\rangle^2(d\Sigma(q)/d\Omega)_c + \langle\Delta\rho\rangle(d\Sigma(q)/d\Omega)_{cf} + (d\Sigma(q)/d\Omega)_f \tag{9}$$

where $(d\Sigma(q)/d\Omega)_c$ is the scattering intensity due to the shape of the sample volume that excludes solvent, $(d\Sigma(q)/d\Omega)_f$ is the scattering intensity from the internal structure of the solvent-excluding parts, and $(d\Sigma(q)/d\Omega)_{cf}$ is the scattering due to the correlation between the shape and the internal structure of the solvent-excluding part of the sample.

The square root of the scattering at "zero angle" $(d\Sigma(0)/d\Omega)^{1/2}$ of a dilute solution of monodisperse particles is proportional to the average contrast $\langle\Delta\rho\rangle$ and is a linear function of scattering length density of solvent $\rho_s$. The extrapolation $(d\Sigma(0)/d\Omega)^{1/2}$ to 0 gives the value of $\rho_s = \langle\rho\rangle$. Deviation from linear dependence of $(d\Sigma(0)/d\Omega)^{1/2}$ vs $\rho_s$ should point on polydispersity of aggregates (composition, size, and shape).

When the average scattering density of particle is obtained, it is possible to analyze the dependence of $R_g$ vs contrast $\langle\Delta\rho\rangle$. According to the contrast variation method, $R_g$ vs $\langle\Delta\rho\rangle$ follows the dependence[25]

$$R_g^2 = R_c^2 + \frac{\alpha}{\langle\Delta\rho\rangle} - \frac{\beta}{\langle\Delta\rho\rangle^2} \tag{10}$$

where $R_c$ is the radius of gyration at infinite contrast and describes the particle shape (homogeneous approximation); coefficients $\alpha$ and $\beta$ are defined by

$$\alpha = V_c^{-1}\int\rho_f(\mathbf{r})r^2\,dv \quad \text{and}$$
$$\beta = V_c^{-2}\int\rho_f(\mathbf{r}_1)\rho_f(\mathbf{r}_2)(\mathbf{r}_1\mathbf{r}_2)\,dv_1\,dv_2 \tag{11}$$

The value of $\alpha$ reflects the distribution the regions of high and low scattering density in particle (if $\alpha > 0$ when lower density region is located in the center of particle and if $\alpha < 0$ when higher density region is in the center). The application of contrast variation and IFT methods in the analysis of SANS data provides information about the overall dimension of structures and the location of different types of material (polymer and metal) inside these structures.

## Results and Discussion

Two different amphiphilic polyethylenimine-amide (PEI-amide) samples, $PEIam5K^{lin}C16_{0.5}$ and $PEIam25K^{lin}C16_{0.5}$, differing in the molecular weight of the

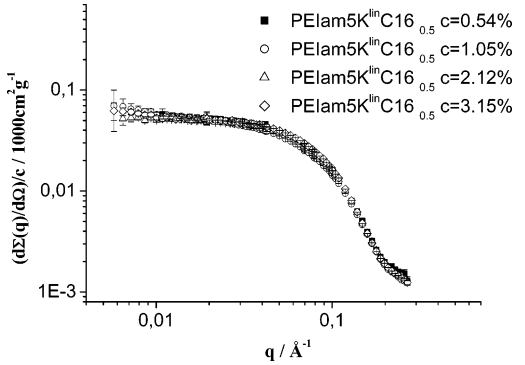


**Figure 1.** SANS intensity for the sample PEIam5K$^{lin}$C16$_{0.5}$ in $C_6D_6$ normalized by concentration.

hyperbranched polyethylenimine scaffold were investigated. SANS on benzene solutions of these polymers demonstrates them to form nonaggregated, inverted unimolecular micelle structures.[22] In short, normalization of the scattering intensity by the polymer concentration leads to an overlap of the different curves indicating that interaction effects are negligible at the concentrations investigated (up to 3.2 wt %; exemplified by Figure 1). The scattering intensity at zero angle, $d\Sigma(0)/d\Omega$, and the radius of gyration $R_g$ of the polymers were obtained within the Guinier approximation and the weight-average molar mass was calculated from the intensity at zero scattering angle as $M_w = (11.9 \pm 1) \times 10^3$ g mol$^{-1}$. This coincides well within experimental error with an $M_w = 13 \times 10^3$ g mol$^{-1}$ calculated from the degree of amidation and average molecular weight of the core ($M_w = 5 \times 10^3$ g mol$^{-1}$) given by the supplier. For the higher molar mass polymer $M_w = (39 \pm 3) \times 10^3$ g mol$^{-1}$ was obtained, which is somewhat less than the value calculated from the average molecular weight of the core ($M_w = 25 \times 10^3$ g mol$^{-1}$ given for this polymer grade). The radius of gyration was 2.3 ± 0.3 nm (PEIam5K$^{lin}$C16$_{0.5}$) and 3.1 ± 0.3 nm (PEIam25K$^{lin}$-C16$_{0.5}$).

**(a) Overall Sizes of Polymer/Ag Particle Hybrids.** The polyethylenimine-amide polymers were employed for the preparation of metal nanoparticles. $AgNO_3$ was solubilized by the polymer in toluene, and the resulting complexed silver ions (polymer/Ag$^+$) were reduced to afford colloidal polymer/Ag-nanoparticle hybrids (polymer/Ag$^{coll}$). The size of the Ag nanoparticles was determined by means of transmission electron microscopy. Particle sizes of 1.2 ± 0.3 and 2.3 ± 0.4 nm were found for the colloids obtained with the low and high molar mass polymer, respectively.

Figure 2 (top) shows SANS data in $C_6D_6$ for systems based on the lower molecular weight polymer. The scattering intensity is significantly higher (4-fold) for the polymer/Ag$^+$ complex (PEIam5K$^{lin}$C16$_{0.5}$/Ag$^+$) and the nanoparticle dispersion (PEIam5K$^{lin}$C16$_{0.5}$/Ag$^{coll}$) compared to solution of the neat polymer (PEIam5K$^{lin}$-C16$_{0.5}$). An upturn of the scattering intensity is observed at lowest $q$ which indicates the presence of some larger aggregates in the solutions, and a trace of scattering from these larger aggregates is observed in lowest $q$ part of the scattering interval. It points to some significant polydispersity due to the metal component; i.e., there are populations of small objects (~5 nm) and of large aggregates (~100 nm). In the data analysis we have analyzed only the interval of $q > 0.02$ Å$^{-1}$ where effects of scattering from large aggregates are negligible. In the bottom part of Figure 2 the same data are given in the

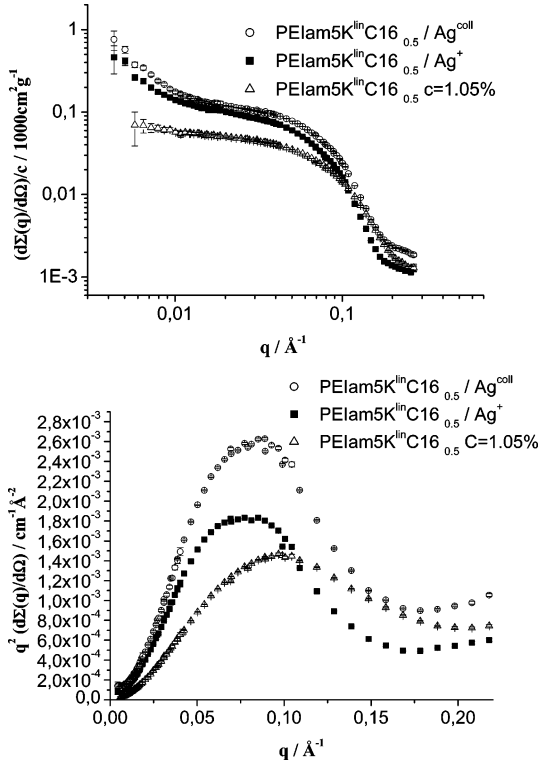


**Figure 2.** SANS data for PEIam5K$^{lin}$C16$_{0.5}$-based samples: neat polymer, polymer + silver salt, and polymer + silver nanoparticles. Top: SANS intensity; bottom: Kratky plot.

form of a Kratky plot, which provides information on the polymer shape. The general shape is the same for all three samples and is typical of hyperbranched polymers. The $q$-position of the maximum is correlated with the mean radius of gyration as $q_{max}R_g = \sqrt{6}$ and shifted to lower $q$ compared to the neat polymer solution. The formation of Ag nanoparticles leads to an increase of the radius of gyration from 2.3 nm for the neat polymer to 4.7 nm for the polymer/Ag$^{coll}$ hybrids.

The equivalent plots for samples based on the higher molecular weight polymer (PEIam25K$^{lin}$C16$_{0.5}$, PEIam25K$^{lin}$-C16$_{0.5}$/Ag$^+$, and PEIam25K$^{lin}$C16$_{0.5}$/Ag$^{coll}$) are shown in Figure 3. The behavior is remarkably different by comparison to the lower molecular weight polymer. The scattering curves reveal no upturn in the low-$q$ region; apparently, this system is more stable toward formation of any aggregates in general. Furthermore, the Kratky plot shows no horizontal shift of the maximum; that is, the average radius of gyration did not change when the metal particles are formed. The obtained radii of gyration are 3.1 nm for the neat polymer (PEIam25K$^{lin}$-C16$_{0.5}$) and 3.3 nm for the polymer/nanoparticle hybrid (PEIam25K$^{lin}$C16$_{0.5}$/Ag$^{coll}$).

The data indicate that for the higher molecular weight polymer the structure is retained upon loading with the silver salt and upon subsequent reduction to silver particles, in terms of a unimolecular "nanoreactor" concept. By contrast, for the lower molecular weight polymer a significant aggregation to larger structures appears to occur upon loading with the silver salt and metal particles synthesis.

**(b) Internal Structure: Local Distribution of Ag Nanoparticles within Polymer/Metal Hybrids.** Contrast variation experiments were performed in order to obtain more detailed information on the internal structures. Figure 4 displays an example of the performed

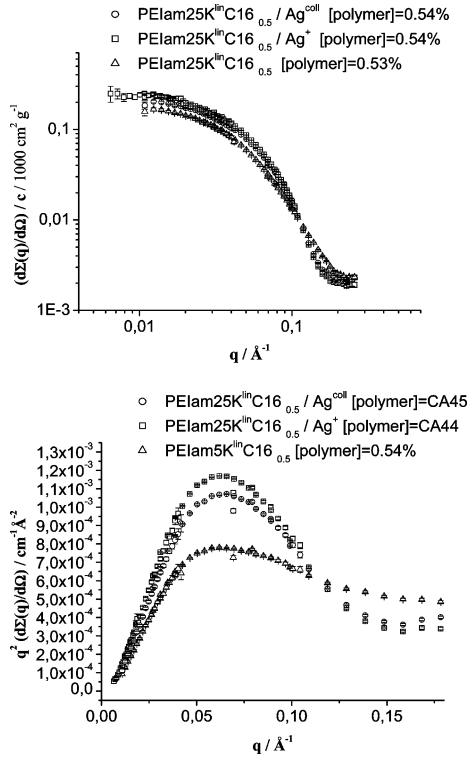


**Figure 3.** SANS data for PEIam25K$^{lin}$C16$_{0.5}$-based samples: neat polymer, polymer + silver salt and polymer + silver nanoparticles, at the same concentration. Top: SANS intensity; bottom: Kratky plot.

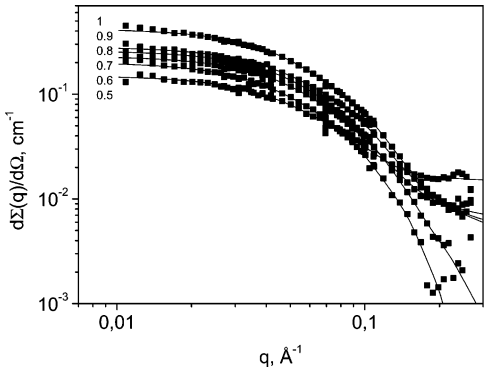


**Figure 4.** SANS data and fits by IFT analysis for PEIam25K$^{lin}$-C16$_{0.5}$ at different contrasts (0.5 wt % polymer; the fraction of $C_6D_6$/$C_6H_6$-mixture is 0.5 to 1 as given in the plot).

analysis, namely, SANS data and fits by IFT analysis for dilute solutions of PEIam25K$^{lin}$C16$_{0.5}$ at different contrasts, i.e., different mixtures of $C_6D_6$ and $C_6H_6$. The total scattering intensity decreases with increasing content of $C_6H_6$, which shows that the neutron scattering length density of PEIam25K$^{lin}$C16$_{0.5}$ macromolecules is less than the scattering length density of $C_6D_6$, as expected. The set of dΣ(0)/dΩ and $R_g$ values obtained from IFT analysis is further analyzed.

The square root of zero-angle scattering $(d\Sigma(0)/d\Omega)^{1}\}^{/2}$ is plotted vs the scattering length density of the solvent for the PEIam5K$^{lin}$C16$_{0.5}$ (top) and for the PEIam25K$^{lin}$-C16$_{0.5}$ (bottom) in Figure 5.

The experimental data follow the linear dependence $(d\Sigma(0)/d\Omega)^{1/2} = A + B\rho_s$, which suggests that the polydispersity of aggregates is within the limit of application of the contrast variation approach, and scattering data of the PEIam5K$^{lin}$C16$_{0.5}$/Ag$^{coll}$ hybrid at $q > 0.02$ Å$^{-1}$ are not disturbed by the presence of larger

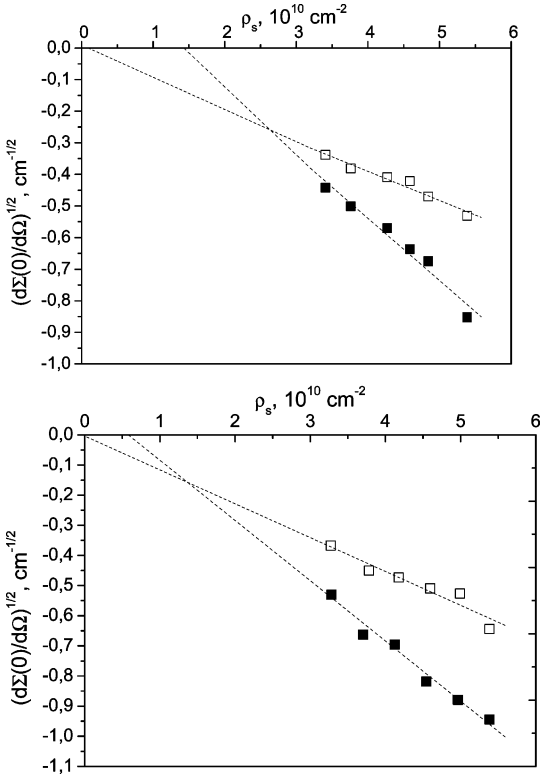


**Figure 5.** Square root of zero-angle scattering vs scattering length density of the solvent. Top: PEIam5K$^{lin}$C16$_{0.5}$ (open symbols) and PEIam5K$^{lin}$C16$_{0.5}$/Ag$^{coll}$ (filled symbols). Bottom: PEIam25K$^{lin}$C16$_{0.5}$ (open symbols) and PEIam25K$^{lin}$-C16$_{0.5}$/Ag$^{coll}$ (filled symbols).

**Table 1. Results of SANS Data Analysis from $(d\Sigma(0)/d\Omega)^{1/2} = A + B\rho_s$**

| | $A$, cm$^{-1/2}$ | $B$, cm$^{3/2}$ × 10$^{-10}$ | ⟨$\rho$⟩, cm$^{-2}$ × 10$^{10}$ |
|---|---|---|---|
| PEIam5K-$^{lin}$C16$_{0.5}$ | 0.00920 ± 0.043 | −0.099 ± 0.0089 | 0.093 ± 0.43 |
| PEIam5K-$^{lin}$C16$_{0.5}$/Ag$^{coll}$ | 0.3 ± 0.025 | −0.209 ± 0.0056 | 1.44 ± 0.35 |
| PEIam25K-$^{lin}$C16$_{0.5}$ | −0.0039 ± 0.01 | −0.112 ± 0.002 | −0.034 ± 0.093 |
| PEIam25K-$^{lin}$C16$_{0.5}$/Ag$^{coll}$ | 0.116 ± 0.0145 | −0.2 ± 0.003 | 0.58 ± 0.07 |

aggregates. The values of fit parameters $A$ and $B$ together with obtained values of average scattering length densities ⟨$\rho$⟩ (from compensation point $((d\Sigma(0)/d\Omega)^{1/2} = 0)$ are presented in Table 1. The absolute value of parameter $B$ (the slope in Figure 5) is proportional to the volume of studied objects. Thus, one can suggest that the presence of silver leads to a size increase of the hybrid vs the neat polymer. The average scattering length density of polymer/Ag hybrids is higher than for neat polymer.

The average scattering length density of polymer/Ag hybrids is connected with ⟨$\rho$⟩ values of neat polymer and neat silver via the volume fraction $\phi$ of polymer in polymer/Ag hybrids as

$$\langle\rho\rangle_{\text{polymer/Ag}} = \phi\langle\rho\rangle_{\text{polymer}} + (1-\phi)\langle\rho\rangle_{\text{Ag}} \qquad (12)$$

where the scattering length density of silver $\langle\rho\rangle_{Ag}$ was calculated from density of the bulk $\langle\rho\rangle_{Ag} = 3.47 \times 10^{10}$ cm$^{-2}$. For PEIam5K$^{lin}$C16$_{0.5}$ in PEIam5K$^{lin}$C16$_{0.5}$/Ag$^{coll}$ hybrids $\phi = 0.60 \pm 0.07$ and for PEIam25K$^{lin}$C16$_{0.5}$ in PEIam25K$^{lin}$C16$_{0.5}$/Ag$^{coll}$ hybrids $\phi = 0.82 \pm 0.08$ were obtained. The fraction of low molecular mass polymer

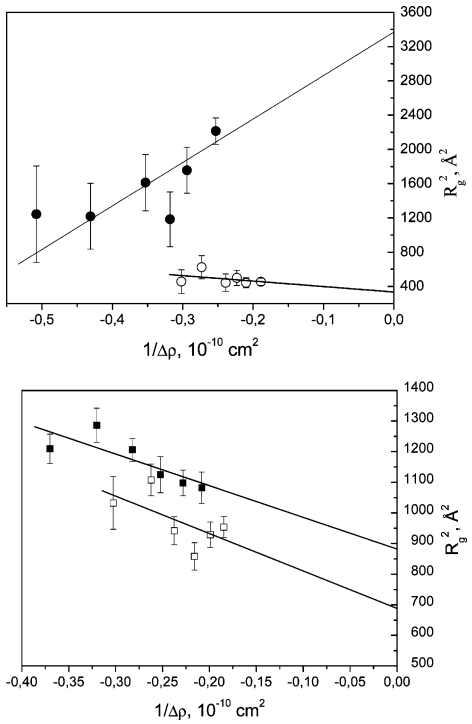


**Figure 6.** Plot of $R_g^2$ vs reciprocal scattering contrast for PEIam5K$^{lin}$C16$_{0.5}$ (top) and PEIam25K$^{lin}$C16$_{0.5}$ (bottom): open symbols, neat polymer; filled symbols, polymer/silver nanoparticles.

**Table 2. Results of SANS Data Analysis from Application of Eq 9**[a]

| | $R_c$, Å | α, $10^{-3}$ |
|---|---|---|
| PEIam5K$^{lin}$C16$_{0.5}$ | 18.1 ± 3.4 | −0.64 ± 0.59 |
| PEIam5K$^{lin}$C16$_{0.5}$/Ag$^{coll}$ | 58.1 ± 4.3 | 5.0 ± 1.6 |
| PEIam25K$^{lin}$C16$_{0.5}$ | 26.2 ± 2.4 | −1.2 ± 0.6 |
| PEIam25K$^{lin}$C16$_{0.5}$/Ag$^{coll}$ | 29.7 ± 1.7 | −1.0 ± 0.4 |

[a] $R_c$ is the radius of gyration at infinite contrast, and α describes the distribution of regions of high and low scattering density within the particle.

is somewhat lower in polymer/Ag complexes as compared to the high molecular weight polymer.

The analysis of $(d\Sigma(0)/d\Omega)^{1/2}$ vs $\rho_s$ provided information about average neutron scattering length density for polymer and polymer/Ag hybrids which was used to obtain the composition of polymer/Ag hybrids. A next step of data analysis concerns the location of Ag inside polymer/Ag hybrids. An analysis of $R_g^2$ vs the inverse scattering contrast $1/\Delta\rho$ according to eq 10 can be carried out. Experimental data are shown in Figure 6. Obviously, PEIam5K$^{lin}$C16$_{0.5}$ and PEIam25K$^{lin}$C16$_{0.5}$ show qualitatively different behavior; i.e., the variation of $R_g^2$ with inverse contrast for neat polymer and polymer/Ag hybrids. Results of the analysis according to eq 9 are listed in Table 2, which provides the radius of gyration at infinite contrast $R_c$ and parameter α which describes the distribution of regions of high and low scattering density within the particle.

The most straightforward situation is encountered for PEIam25K$^{lin}$C16$_{0.5}$ (Figure 6, bottom). Both for the neat polymer and the polymer/nanoparticle hybrids (samples PEIam25K$^{lin}$C16$_{0.5}$ and PEIam25K$^{lin}$C16$_{0.5}$/Ag$^{coll}$) the values of parameter α are equal within statistical errors (Table 2) and the slope is negative. This means that the scattering density is slightly higher in the center of the particle, which is typical of polymers. It reveals that the presence of Ag does not change the overall distribution of scattering length density which should reflect the homogeneous distribution of Ag particles within PEIam25K$^{lin}$C16$_{0.5}$/Ag$^{coll}$ hybrids. Also, the absolute value of α is close to zero (2 times larger than statistical errors), which shows that the difference in scattering length density in center and periphery of the objects is small; thus, PEIam25K$^{lin}$C16$_{0.5}$ and PEIam25K$^{lin}$C16$_{0.5}$/Ag$^{coll}$ are quite homogeneous.

A different behavior is found for the lower molecular weight sample (see Figure 6, top). For the neat polymer (PEIam5K$^{lin}$C16$_{0.5}$), the slope is negative and the value of α is very close to zero, as expected for polymeric structures that are mostly homogeneous. However, a positive slope and high value of α which is significantly larger than zero are observed for the PEIam5K$^{lin}$C16$_{0.5}$/Ag$^{coll}$ hybrid. A first straightforward conclusion is that Ag nanoparticles are distributed inhomogeneously within PEIam5K$^{lin}$C16$_{0.5}$/Ag$^{coll}$ hybrids because the values of α are different in sign and magnitude for PEIam5K$^{lin}$C16$_{0.5}$ and PEIam5K$^{lin}$C16$_{0.5}$/Ag$^{coll}$ hybrids, which is totally opposite to the behavior found with the higher molecular weight polymer PEIam25K$^{lin}$C16$_{0.5}$ and corresponding colloids.

In more detail, the regions with higher scattering density are located on the periphery of PEIam5K$^{lin}$C16$_{0.5}$/Ag$^{coll}$ hybrids. This indicates that the Ag metal particles are not located in the center but rather on the outside of these structures.

The difference in the slope and sign of the parameter α between the two samples agrees with the different behavior observed with the radius of gyration (previous section a). As mentioned above, $R_g$ of the PEIam25K$^{lin}$C16$_{0.5}$ sample did not change significantly when Ag nanoparticles were present, whereas the radius of gyration of the PEIam5K$^{lin}$C16$_{0.5}$ sample increased vs the neat polymer when Ag particles have been formed. An increase of $R_g$ is expected when the metal particle is located off-center, whereas $R_g$ should not increase when the Ag particle is homogeneously distributed within the macromolecule.

Obviously, a significant difference is observed with the two polymers of different molar masses. With the larger polymer, the Ag nanoparticles seem to be incorporated inside the macromolecules near the center of gravity (Scheme 1). The observation that the metal nanoparticles are located off-center in the case of the low molar mass polymer indicates the smaller macromolecules are not able to embed the metal particle homogeneously. This behavior can be related to the findings of Amis et al. for the case of the formation of gold nanoparticles in the presence of nonamphiphilic dendrimers.[9] They observed for generations G6 to G9 that one metal particle was formed in one den drimer molecule and that it was located offset from the center.

We can only speculate on the aggregate structure in the case of the polymer/metal particle hybrides formed by the lower molecular weight polymer (PEIam5K$^{lin}$C16$_{0.5}$/Ag$^{coll}$). One possibility is that the aggregate consists of several polymer molecules and metal particles that are inhomogeneously distributed within the aggregate. A single metal nanoparticle may also be encapsulated by several polymer molecules and be located offset from the center. In both cases, the aggregation is a consequence of an insufficient shielding of the polar scaffolds by the apolar core of the small

**Scheme 1. Schematic Representation of Particle Synthesis and the Structure of the Resulting Amphiphilic Polymer/Silver Nanoparticle Hybrid for the Larger Polyethylenimine Core**[a]

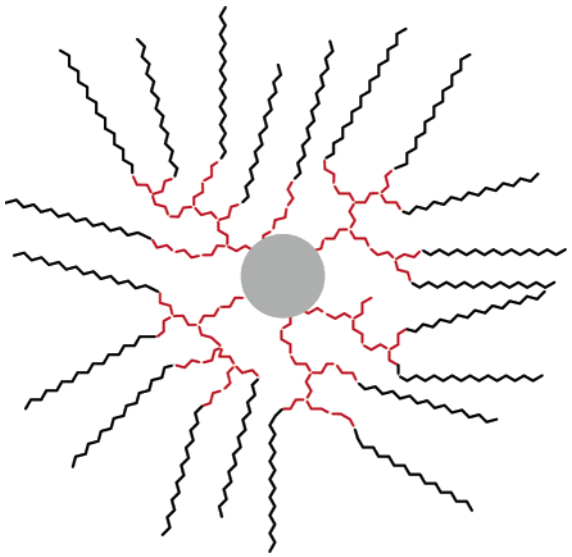

[a] Gray = core; black = fatty acid side chains.

polymer, in contrast to a more efficient shielding in the larger more flexible macromolecules.

## Summary and Conclusions

SANS measurements of amphiphilic polyethylenimine-amide/silver nanoparticle hybrides and of the metal salt-loaded polymer/$Ag^+$ complexes reveal no significant structural changes compared to the neat polymer when a polymer of $M_w$ 39 × $10^3$ g $mol^{-1}$ is employed. This is in accordance with the synthesis of a single metal particle in a nanoreactor consisting of an inverted unimolecular micelle. By contrast, for a lower molecular weight polymer with a smaller polar scaffold ($M_w$ 12 × $10^3$ g $mol^{-1}$), some degree of aggregation is observed upon metal salt loading and also in the final polymer/metal particle hybrid.

Contrast variation experiments in solvent mixtures with varying $C_6D_6/C_6H_6$ ratios provide information on the internal structure that is particularly on the local distribution of the polymer and of the Ag particles within the polymer/metal particle hybrids. The samples based on the higher molecular weight polymer display a scattering length density typical for a distribution homogeneous with respect to the center of mass. By contrast, for the lower molecular weight polymer the silver particles are off-center and rather located on the periphery of the aggregates formed.

In summary, amphiphilic hyperbranched polymers which are easily accessible on a kilogram scale can serve as molecular confined environments for the synthesis and stabilization of inorganic metal particles.

**Acknowledgment.** This work was supported by the VolkswagenStiftung (Schwerpunkt "Komplexe Materialien"). Funding by the DFG (SFB 428) is acknowledged. S.M. is indebted to the Fonds der Chemischen Industrie and to the Hermann-Schnell-Foundation for financial support.

**Supporting Information Available:** TEM micrographs and histograms of silver colloids; polymer solution densities. This material is available free of charge via the Internet at http://pubs.acs.org.

## References and Notes

(1) (a) Faraday, M. *Philos. Trans. R. Soc. London* **1857**, *147*, 145−181. (b) Ostwald, W. *Die Welt der vernachlässigten Dimensionen*; Steinkopff: Dresden, 1915. (c) Rampino, L. D.; Nord, F. F. *J. Am. Chem. Soc.* **1941**, *63*, 2745−2749.

(2) (a) Reetz, M. T.; Helbig, W. *J. Am. Chem. Soc.* **1994**, *116*, 7401−7402. (b) Reetz, M. T.; Winter, M.; Breinbauer, R.; Thurn-Albrecht, T.; Vogel, W. *Chem.−Eur. J.* **2001**, *7*, 1084−1094. (c) Bredig, G. *Z. Angew. Chem.* **1898**, *10*, 951−954. (d) Rodríguez-Sánchez, L.; Blanco, M. C.; López-Quintela, M. A. *J. Phys. Chem. B* **2000**, *104*, 9683−9688.

(3) (a) Hess, P. H.; Parker, P. H., Jr. *J. Appl. Polym. Sci.* **1966**, *10*, 1915−1927. (b) Chan, Y. N. C.; Schrock, R. R.; Cohen, R. E. *Chem. Mater.* **1992**, *4*, 24−27. (c) Duteil, A.; Quéau, R.; Chaudret, B.; Mazel, R.; Roucau, C.; Bradley, J. S. *Chem. Mater.* **1993**, *5*, 341−347. (d) Ould Ely, T.; Pan, C.; Amiens, C.; Chaudret, B.; Dassenoy, F.; Lecante, P.; Casanove, M.-J.; Mosset, A.; Respaud, M.; Broto, J.-M. *J. Phys. Chem. B* **2000**, *104*, 695−702. (e) Choukroun, R.; de Caro, D.; Chaudret, B.; Lecante, P.; Snoeck, E. *New J. Chem.* **2001**, *25*, 525−527.

(4) (a) Kurihara, K.; Fendler, J. H. *J. Am. Chem. Soc.* **1983**, *105*, 6152−6153. (b) Kurihara, K.; Fendler, J. H.; Ravet, I.; Nagy, J. B. *J. Mol. Catal.* **1986**, *34*, 325−335. (c) Toshima, N.; Takahashi, T.; Hirai, H. *Chem. Lett.* **1986**, 35−38. (d) Toshima, N.; Takahashi, T.; Hirai, H. *Chem. Lett.* **1987**, 1031−1034.

(5) (a) Ng Cheong Chan, Y.; Craig, G. S. W.; Schrock, R. R.; Cohen, R. E. *Chem. Mater.* **1992**, *4*, 885−894. (b) Saito, R.; Okamura, S.; Ishizu, K. *Polymer* **1992**, *33*, 1099−1101. (c) Antonietti, M.; Wenz, E.; Bronstein, L.; Seregina, M. *Adv. Mater.* **1995**, *7*, 1000−1005. (d) Spatz, J. P.; Roescher, A.; Moeller, M. *Adv. Mater.* **1996**, *8*, 337−340. (e) Moffitt, M.; Eisenberg, A. *Chem. Mater.* **1995**, *7*, 1178−84. (f) Moeller, M.; Spatz, J. P. *Curr. Opin. Colloid Interface Sci.* **1997**, *2*, 177−187. (g) Bronstein, L.; Antonietti, M.; Valetsky, P. In *Nanoparticles and Nanostructured Films*; Fendler, J. H., Ed.; Wiley-VCH: Weinheim, 1998; pp 145−71.

(6) Mössmer, S.; Spatz, J. P.; Möller, M.; Aberle, T.; Schmidt, J.; Burchard, W. *Macromolecules* **2000**, *33*, 4791−4798.

(7) (a) Zhao, M.; Sun, L.; Crooks, R. M. *J. Am. Chem. Soc.* **1998**, *120*, 4877−4878. (b) Balogh, L.; Tomalia, D. A. *J. Am. Chem. Soc.* **1998**, *120*, 7355−7356. (c) Esumi, K.; Suzuki, A.; Aihara, N.; Usui, K.; Torigoe, K. *Langmuir* **1998**, *14*, 3157−3159.

(8) Cölfen, H. *Macromol. Rapid Commun.* **2001**, *22*, 219−252.

(9) Gröhn, F.; Bauer, B. J.; Akpalu, Y. A.; Jackson, C. L.; Amis, E. J. *Macromolecules* **2000**, *33*, 6042−6050.

(10) (a) Fischer, M.; Vögtle, F. *Angew. Chem., Int. Ed.* **1999**, *38*, 885−905; *Angew. Chem.* **1999**, *111*, 934−955. (b) Bosman, A. W.; Janssen, H. M.; Meijer, E. W. *Chem. Rev.* **1999**, *99*, 1665−1688. (c) Hecht, S.; Fréchet, J. M. J. *Angew. Chem., Int. Ed.* **2001**, *40*, 74−91; *Angew. Chem.* **2001**, *113*, 76−94. (d) Oosterom, G. E.; Reek, J. N. H.; Kamer, P. C. J.; van Leeuwen, P. W. N. M. *Angew. Chem., Int. Ed.* **2001**, *40*, 1828−1849; *Angew. Chem.* **2001**, *113*, 1878−901. (e) Daniel, M. C.; Astruc, D. *Chem. Rev.* **2004**, *104*, 293−346.

(11) (a) Flory, P. J. *J. Am. Chem. Soc.* **1952**, *74*, 2718−2723. (b) Voit, B. I. *Acta Polym.* **1995**, *46*, 87−99. (c) Kim, Y. H. *J. Polym. Sci., Polym. Chem. Ed.* **1998**, *36*, 1685−1698. (d) Sunder, A.; Heinemann, J.; Frey, H. *Chem.−Eur. J.* **2000**, *6*, 2499−2506.

(12) Linear polymer: DB 0%, calculated according to DB = 2*D*/(2*D* + *L*), *D* = dendritic units (tertiary amine), *L* = linear units (secondary amine). Cf. Hölter, D.; Burgath, A.; Frey, H. *Acta Polym.* **1997**, *48*, 30−35.

(13) (a) Sunder, A.; Hanselmann, R.; Frey, H.; Mülhaupt, R. *Macromolecules* **1999**, *32*, 4240−4246. (b) Product information brochure hyperpolymers GmbH, www.hyperpolymers.com.

(14) Product information brochure Lupasol, BASF AG.

(15) Stevelmans, S.; van Hest, J. C. M.; Jansen, J. F. G. A.; van Boxtel, D. A. F. J.; de Brabander-van den Berg, E. M. M.; Meijer, E. W. *J. Am. Chem. Soc.* **1996**, *118*, 7398−7399.

(16) (a) Chechik, V.; Zhao, M.; Crooks, R. M. *J. Am. Chem. Soc.* **1999**, *121*, 4910−4911. (b) Chechik, V.; Crooks, R. M. *J. Am. Chem. Soc.* **2000**, *122*, 1243−1244.

(17) (a) Sunder, A.; Krämer, M.; Hanselmann, R.; Mülhaupt, R.; Frey, H. *Angew. Chem., Int. Ed.* **1999**, *38*, 3552−3554. (b) Stiriba, S.-E.; Kautz, H.; Frey, H. *J. Am. Chem. Soc.* **2002**, *124*, 9698−9699.
(18) (a) Mecking, S.; Thomann, R.; Frey, H.; Sunder, A. *Macromolecules* **2000**, *33*, 3958−3960. (b) Mecking, S.; Schlotterbeck, U.; Thomann, R.; Soddemann, M.; Stieger, M.; Richtering, W.; Kautz, H. *Polym. Mater. Sci. Eng.* **2001**, *84* , 511−512.
(19) Sablong, R.; Schlotterbeck, U.; Vogt, D.; Mecking, S. *Adv. Synth. Catal.* **2003**, *345*, 333−336.
(20) Schlotterbeck, U.; Aymonier, C.; Thomann, R.; Hofmeister, H.; Tromp, M.; Richtering, W.; Mecking, S. *Adv. Funct. Mater.*, in press.
(21) Aymonier, C.; Schlotterbeck, U.; Antonietti, L.; Zacharias, P.; Thomann, R.; Tiller, J. C.; Mecking, S. *Chem. Commun.* **2002**, 3018−3019.
(22) Antonietti, L.; Aymonier, C.; Schlotterbeck, U.; Thomann, R.; Maksimova, T.; Richtering, W.; Mecking, S., manuscript in preparation.
(23) Stuhrmann, H. B.; Burkhardt, N.; Dietrich, G.; Jünemann, R.; Meerwinck, W.; Schmitt, M.; Wadzack, J.; Willumeit, R.; Zhao, J.; Nierhaus, K. H. *Nucl. Instrum. Methods* **1995**, *A356*, 133−137.
(24) Wignall, G. D.; Bates, F. S. *J. Appl. Crystallogr.* **1986**, *20*, 28.
(25) Pedersen, J. S.; Posselt, D.; Mortensen, K. *J. Appl. Crystallogr.* **1990**, *23*, 321.
(26) Bevington, B. R. *Data Reduction and Error Analysis for Physical Sciences*; McGraw-Hill: New York, 1969.
(27) Burchard, W. *Macromolecules* **1977**, *10*, 919.
(28) deLuca, E.; Richards, R. W.; Grillo, I.; King, S. M. *J. Polym. Sci., Part B: Polym. Phys.* **2003**, *41*, 1352−1361.
(29) Stuhrmann, H. B.; Kirste, R. G. *Z. Phys. Chem. (Munich)* **1967**, *56*, 334−341.
(30) Pedersen, J. S. *Adv. Colloid Interface Sci.* **1997**, *70*, 171.
(31) Glatter, O. *J. Appl. Crystallogr.* **1977**, *10*, 415.
(32) Glatter, O. In *International Tables for Crystalography*; Wilson, A. J. C., Eds.; Kluwer Academic Publishers: Dordrecht, 1992; Vol. C, pp 89−105.

MA048965G